

# Implicit Object Mapping With Noisy Data

Jad Abou-Chakra, Feras Dayoub, and Niko Sünderhauf

**Abstract**—Modelling individual objects as Neural Radiance Fields (NeRFs) within a robotic context can benefit many downstream tasks such as scene understanding and object manipulation. However, real-world training data collected by a robot deviate from the ideal in several key aspects. (i) The trajectories are constrained and full visual coverage is not guaranteed – especially when obstructions are present. (ii) The poses associated with the images are noisy. (iii) The objects are not easily isolated from the background. This paper addresses the above three points and uses the outputs of an object-based SLAM system to bound objects in the scene with coarse primitives and – in concert with instance masks – identify obstructions in the training images. Objects are therefore automatically bounded, and non-relevant geometry is excluded from the NeRF representation. The method’s performance is benchmarked under ideal conditions and tested against errors in the poses and instance masks. Our results show that object-based NeRFs are robust to pose variations but sensitive to the quality of the instance masks.

## I. INTRODUCTION

Robots that construct semantically meaningful maps rich with geometric data can better facilitate decision making and control tasks [1], [2]. Finding expressive representations that would populate such a map is a critical stepping stone towards increasing the utility and flexibility of robots.

Classical simultaneous localization and mapping systems (SLAM) model the world with varying degrees of fidelity and detail. They produce basic maps composed of primitives like points [3], surfels [4], or voxels [5]. Object-based variants of these inject some semantics into the map by identifying and bounding objects within quadrics [6] or cubes [7]. Despite adding a semantic dimension, object-based SLAM does not capture the geometry and radiance of the objects and therefore has limited use. Finding a reliable and rich object representation that can be extracted by a robot from typically noisy data is an ongoing challenge [1], [8], [9]. Neural Radiance Fields (NeRFs) [10] are recent advancements in implicit representations that have become popular due to their remarkable success on the view-synthesis task. This representation of 3D scenes is learnt from well-posed images and produces photo-realistic renders from novel viewpoints. In this paper, we show how NeRFs can be used as object rather than scene representations and analyze their sensitivity to noisy and constrained input typical of robotic applications.

We demonstrate that NeRFs are a natural extension to object-based SLAM systems and that they are complimentary – one provides tractability and the other accuracy. NeRFs are neural networks that are trained with posed images and represent a manually configured area with high fidelity. In contrast, object-based SLAM lacks geometric fidelity but is capable of quickly associating input images with poses and

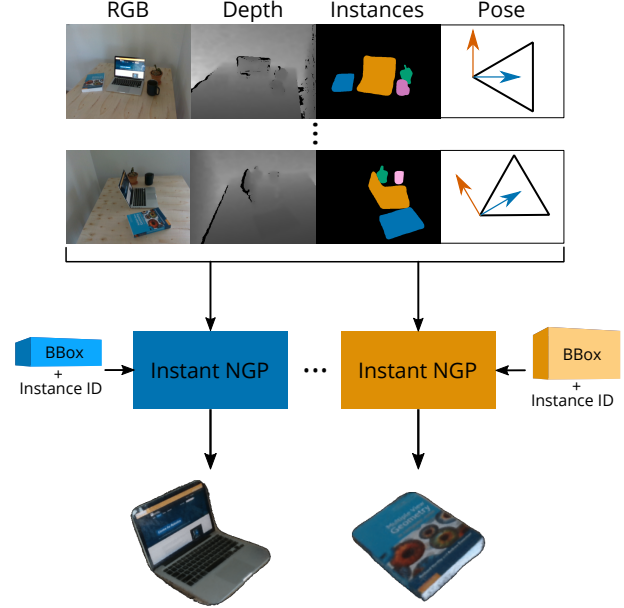


Fig. 1. We generate a neural radiance field (NeRF) with a hash encoding (Instant NGP) for each object in the scene. We use noisy instance masks and loose bounding boxes – assumed to be provided by an object-based SLAM system – to bound each NeRF and isolate the object from its background. A scene with 4 objects can thus be decomposed into 4 NeRFs, each representing the geometry of a single object.

automatically detecting areas of interest in a scene. Using the two systems in concert to remove the disadvantages of either is the approach we take in this paper. We present such a method and investigate how well it performs under constraints and noise typical in robotic contexts.

The robotic context of the semantic mapping problem imposes restrictions on using NeRFs. A large number of well-posed and well-distributed views with overlapping frustums would ideally be used to train a NeRF. In a robotic use case, these ideals may not be met – trajectories may be constrained and the poses calculated are of varying precision and accuracy. In addition, NeRFs are designed to model scenes and not the individual objects within. Modelling objects requires a strategy of isolating them and of suppressing the inclusion of geometry that does not belong to them.

Our contributions are as follows:

- We present a method of creating object NeRFs that is facilitated by typical outputs from an object-based SLAM system
- We baseline the method’s performance on an ideal dataset and show how it deteriorates when the camera trajectory is constrained and when the instance masks

and extrinsics are noisy.

## II. RELATED WORK

### A. Object-based SLAM

Object-based SLAM systems [6], [7], [11], [12] use objects in the scene as landmarks to estimate their pose as well as that of the camera's. They generate semantically meaningful maps which are populated by objects of interest. This is in contrast to purely geometric SLAM systems [3]–[5] which use points, surfels, or voxels as the mapped element. QuadricSLAM [6] and CubeSLAM [7] are notable examples of object-based SLAM that model objects as quadrics and cubes respectively. In both cases, the mapping element is a coarse primitive that belies the complexity of the geometry within. While the simplicity of the primitives is what allows real-time operation, it also handicaps downstream tasks which may require more precise knowledge of the objects discovered.

### B. Implicit Representations

Implicit representations [10], [13], [14] compactly capture geometry in continuous functions. Neural radiance fields are examples of these. Mildenhall et al. [10] show that training a multi-layered perceptron (MLP) to represent the radiance field of a scene allows the rendering of photo-realistic images on novel views. This original incarnation of NeRFs assumes the scene being mapped is bounded, and that the training images are from cameras pointed at roughly the same target and distributed along a hemisphere. The method used to formulate and encode the inputs have a large impact on rendering and training speed. Among those works that target inference [15]–[17] and training time [18], [19], Instant-NGP [20] is the only one that does both. This makes it the most suitable for robotic applications. It does this by introducing hash encodings which allows the underlying MLP to become much smaller.

In this paper, we are interested in creating object representations with NeRFs. Prior work in this domain [21]–[23] make strong assumptions of fixed backgrounds and ideal instance masks that are unsuitable for robotics. Our paper enumerates and quantifies the challenges of using NeRFs as object representations “in the wild” under the influence of constraints and noise usually present in robotic applications. NeRF-based models are being used for mapping [24] and manipulation [25]–[27]. Object-based variations [26], [28] are likely to become increasingly important for these use-cases.

## III. PRELIMINARY

A NeRF is a continuous representation of a 3D scene that maps a point  $\mathbf{x}_i \in \mathbb{R}^3$  and a view direction  $\mathbf{d}_i \in \mathbb{S}^2$  to a colour  $\mathbf{c}_i \in \mathbb{R}^3$  and a density value  $\sigma_i \in \mathbb{R}$ . NeRFs are trained by casting rays from a camera center through the image plane and progressively sampling points along them. A ray is parameterized as  $\mathbf{r}(t) = \mathbf{o} + t\mathbf{d}$  where  $\mathbf{o} \in \mathbb{R}^3$  is the ray origin and  $\mathbf{d} \in \mathbb{S}^2$  is the ray direction. Sampling  $N + 1$  points along the ray and defining  $\delta_i = t_{i+1} - t_i$  for



Fig. 2. Each training image can be decomposed into three regions through which rays are cast: (i) Rays cast through the positive region – shown as green – represent the object and have their computed color optimized towards the groundtruth color in the image. (ii) Rays cast through the negative region – shown as random colors – represent the background and are optimized towards a zero density distribution. (iii) Rays cast through the masked region – shown in pink – represent possible obstructions and are not included in the training.

$i \in [0, N]$ , the expected ray colour  $\hat{C}(\mathbf{r})$  and the expected distance a ray will travel  $\hat{D}(\mathbf{r})$  are given by:

$$\hat{C}(\mathbf{r}) = \sum_{i=1}^N w_i \mathbf{c}_i \quad \text{and} \quad \hat{D}(\mathbf{r}) = \sum_{i=1}^N w_i t_i$$

where  $w_i = T_i(1 - \exp(-\sigma_i \delta_i))$  and  $T_i = \exp(-\sum_{j=1}^{i-1} \sigma_j \delta_j)$

(1)

## IV. METHOD

The approach we take in this paper in pursuit of a rich and semantically meaningful map is to assume the presence of an object-based SLAM system that localises the camera, identifies objects in the scene, and bounds them using a coarse primitive. We present a method that extends this system and enriches its representation of objects through the use of Neural Radiance Fields (NeRFs). Given a set of images  $I_i$  and their corresponding poses  $X_i$ , depth maps  $D_i$ , and instance masks  $S_i$ , we aim to construct a single NeRF for every object  $j$  present in the scene. A ray  $\mathbf{r}$  that intersects an image plane  $i$  at a pixel coordinate  $(u, v)$  is associated with the color  $\mathbf{c}_{gt}(\mathbf{r}) = I_i(u, v)$ , the depth  $d_{gt}(\mathbf{r}) = D_i(u, v)$ , and the instance ID  $S_i(u, v)$ .

The object-centric nature of the task presents challenges that do not appear when mapping whole scenes. The first challenge is bounding the NeRF to an area so that its representational power can be focused on the object of interest. In this, we rely on the object-based SLAM system to provide a bounding box  $B_j$  that loosely contains the object. We use a ray-box intersection algorithm to ignore rays that do not pass through the bounding box and to limit sampling to the points therein.



Fig. 3. Renders from four object NeRFs extracted from a real scene show various geometry artifacts that may be due to insufficient view coverage, noisy instance masks, and inaccuracies in the poses. The training data is taken from a constrained trajectory and instance masks are produced by MaskRCNN. Depth supervision is not used in this example. Large simple geometries – as seen in the laptop and book renders – are reconstructed more accurately than their counterparts. In general, the objects are well-isolated from their background, however attributing the artifacts to different sources of error is difficult in real scenes. This begs the question: “To what extent does each noise factor contribute to imperfections in the NeRF?”

The second challenge is to isolate that object in the presence of clutter. The aim is to construct the object while suppressing any other geometry around it. To this end, rays that are known to hit the object should encourage geometry to be formed along them. Conversely, rays that do not hit the object should discourage it. Rays that are obstructed from hitting the object by another are not included in the training because their groundtruth values are not known – the colors that correspond to them are not of the object of interest but rather of the object that is obstructing it. Therefore, rays are cast from each training image through three different regions (illustrated in Figure 2): (i) the negative region – corresponding to the background – that discourages geometry formation, (ii) the positive region – corresponding to the object – that promotes it, and (iii) the masked region – corresponding to potential obstacles – that does neither. The rays  $\mathcal{R}_p$  cast through positive regions are given groundtruth targets from the training images as is done in conventional NeRF training. They are identified as those rays that have a corresponding instance ID equal to the object’s ID. The rays  $\mathcal{R}_m$  passing through the masked region have no influence on training. These are the rays whose associated instance ID belong to an object other than the one being mapped and intersect that object’s bounding box before intersecting the NeRF’s. The remaining rays  $\mathcal{R}_n$  are the ones cast through the negative regions. If every point on one such ray has a density of 0, the rendered color would be  $\mathbf{0}$  (black). The inverse, however, is not true. Therefore, to avoid the edge case of creating black geometry instead of no geometry, the rays are given a constantly changing colour target to encourage the densities towards zero and the colors away from it (as is done in [20]). This method assumes that the geometries obstructing the training views are recognized by the instance masks and the object-based SLAM systems.

Our final photometric loss is formulated as:

$$L_{rgb} = \sum_{\mathbf{r} \in \mathcal{R}} \|e_{rgb}\|_2 \quad (2)$$

where

$$e_{rgb}(\mathbf{r}) = \begin{cases} \hat{C}(\mathbf{r}) - \mathbf{c}_{gt}(\mathbf{r}) & \text{if } \mathbf{r} \in \mathcal{R}_p \\ \hat{C}(\mathbf{r}) - \mathbf{c}_{random} & \text{if } \mathbf{r} \in \mathcal{R}_n \\ 0 & \text{if } \mathbf{r} \in \mathcal{R}_m \end{cases} \quad (3)$$

$\mathcal{R}$  is the set of all rays that pass through the training images.  $\mathbf{c}_{gt}(\mathbf{r})$  is the color of the pixel in the training image that the ray  $\mathbf{r}$  intersects.  $\mathbf{c}_{random}$  is a vector drawn from a uniform distribution  $U(0, 1)$ .

**Depth Supervision:** It is relatively inexpensive to fit an RGBD camera to a robot. The extra information is incorporated into the training by including a depth loss  $L_{depth}$  which is only applied to rays that have a valid groundtruth depth, a low total accumulated transmittance and belong to  $\mathcal{R}_p$ . In this way, depth only corrects geometry that has been already been created and has less influence on whether that geometry should be formed or suppressed. This makes the method more robust to noisy depth maps. We use an L1 loss because it results in sharper reconstructions with density distributions along the ray that have low entropy.

$$L_{depth} = \sum_{\mathbf{r} \in \mathcal{R}} |e_{depth}| \quad (4)$$

where

$$e_{depth}(\mathbf{r}) = \begin{cases} \hat{D}(\mathbf{r}) - \mathbf{d}_{gt}(\mathbf{r}) & \text{if } \mathbf{r} \in \mathcal{R}_p, T_N < 10^{-4}, \\ & \text{and } \mathbf{d}_{gt}(\mathbf{r}) > 0 \\ 0 & \text{otherwise} \end{cases} \quad (5)$$

The method is not sensitive to the empirically chosen threshold condition  $T_N < 1e^{-4}$ .

**Joint Optimization:** The learnable parameters  $\Phi$  of the NeRF framework and the poses  $X$  of the cameras are jointly





Fig. 4. A real scene with four objects of interest is explored by a camera moving along a constrained trajectory – shown in blue. The path is calculated by ORBSLAM [29] as is typical for many robotic applications. Object NeRFs extracted from this scene must contend with the limited viewpoints afforded by the trajectory, the objects obstructing each other, and noise in the computed poses and instance masks.

optimized.

$$\Phi^*, X^* = \arg \min_{\Phi, X} L_{rgb} + w_{depth} L_{depth} \quad (6)$$

**Implementation Details:** Instant-NGP [20] with a multi-resolution hash encoding is used as the underlying NeRF model because it trains in close to real-time making it the most suitable for robotic applications. Furthermore, the implementation released by the authors provides much of the functionality needed to implement this paper including extrinsics optimization and ray-box intersections. The implementation is extended to add support for a depth loss and to isolate objects based on an instance ID found in the masks. For details on Instant-NGP itself and its hash encoding, the reader is referred to [20]. The Instant-NGP configuration used is described in Table I. The authors of [20] optimize each training pose with Adam [30] configured with  $\beta_1 = 0.9$ ,  $\beta_2 = 0.99$ ,  $\epsilon = 10^{-9}$ . The learning rate is exponentially decayed from  $3.3 \cdot 10^{-4}$  to  $10^{-5}$ . All models are trained for 2000 steps.  $w_{depth} = 3.0$  when the depth loss is included.

## V. EVALUATION

The method is run on the real scene shown in Figure 4 and qualitative data is collected and shown in Figure 3. An Intel D435 camera is used to capture 100 images along a constrained trajectory. In the absence of a robust open-source implementation of object-based SLAM, loose bounding boxes are manually estimated around objects in the scene and camera positions are initialized with ORBSLAM3 [29] – an odometry system that can underpin QuadricSLAM [6] and CubeSLAM [7] and is therefore a lower bound on accuracies expected. Lastly, instance masks are given by

MaskRCNN [31]. The reconstruction quality is affected by many factors including the size and geometry of objects, their visibility to the cameras in the trajectory, the noise in the poses and the noise in the instance masks. Because groundtruth data is unavailable when using real-world data, it is difficult to quantitatively assess the method. Therefore, we construct a series of experiments on synthetic datasets to evaluate the method’s sensitivity to these factors. Section V-A begins by determining an upper bound on reconstruction quality in ideal conditions. Section V-B studies the affect of noisy instance masks. Section V-C analyzes the robustness to increasing inaccuracies in camera poses. Lastly, section V-D measures the method’s performance on a cluttered scene and a constrained trajectory similar to the real scene in 4.

**Metrics** The shape of an object is the most important facet of object mapping for the purposes of informing robotic tasks. In contrast to those works that use NeRFs for novel view synthesis, we evaluate primarily on the accuracy of the geometry rather than that of the color. In this, there is a difficulty that is introduced by the semantic aspect of the problem. We differentiate between areas which have been correctly categorized as part of the object of interest and areas which have not. For correctly categorized areas, we use the mean average depth error (MAE) between the groundtruth and rendered depth maps to measure accuracy. We also use an intersection-over-union (IoU) between the ideal and rendered instance masks to measure how much of the total shape is represented in the NeRF.

**Datasets** Datasets used in the experiments below are derived from the Blender Cube Diorama scene [32]. The Blender scene is packaged with a number of assets that make it easy to conduct controlled experiments with groundtruth data and for others to recreate the experiments. We test on four objects “Laptop”, “Tea Cup”, “Bluebell”, and “Book”. These are shown in Figure 6. The particular items are chosen because they can also be segmented by MaskRCNN [31] pre-trained on the MS COCO dataset [33]. The models vary in shape and size and present different challenges to the training. The “Bluebell” model, for example, is composed of many thin structures, whereas the “Tea Cup” is relatively small and has a hard to learn cavity. All images have a resolution of 640x480.

### A. Baseline

Before evaluating the effect of various noise levels on NeRF training, a baseline is established in an ideal scene with perfect data and well-distributed cameras. Four scenes are constructed; each having an object from Figure 6 placed on a table. A NeRF is trained using a set of images and instance masks taken from the top half of a sphere looking at the center of the object. We show how increasing the number of views, utilizing a depth loss, and changing the distance between the object and the cameras affects the reconstruction. The average depth error and the IoU are measured across a test set of 50 novel views from the same top hemisphere.

TABLE I  
INSTANT-NGP NETWORK CONFIGURATION

Parameter	Value
Number of levels	16
Hash table size	$2^{19}$
Number of feature dimensions per entry	2
Coarsest resolution	16
Finest resolution	2048

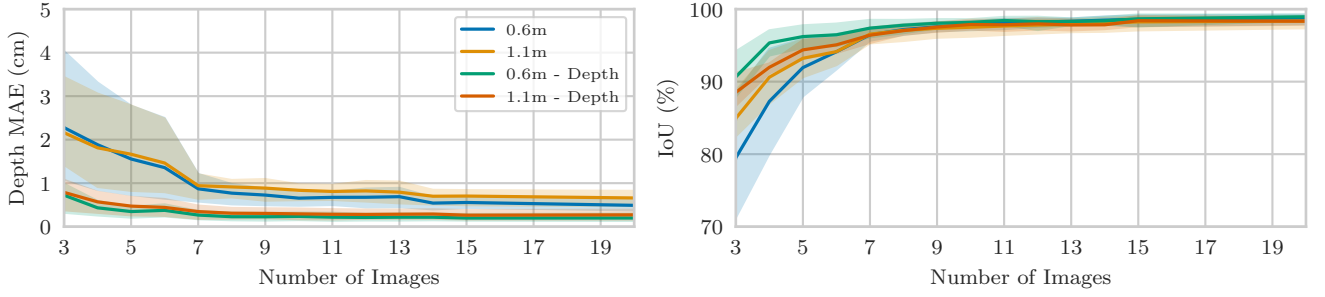


Fig. 5. NeRFs – representing one of four tabletop objects placed in an indoor scene – are trained from an increasing number of well-distributed posed images with groundtruth instance masks. The images are taken from the top half of a sphere with radius 0.6m and 1.1m. Depth supervision is enabled for two of the experiments. The tabletop objects can be reconstructed with an accuracy under 1 cm at 98% IoU. The number of training images has a diminishing effect on the quality of the reconstruction whereas depth supervision gives an overall increase in accuracy ( $< 0.5$  cm at 98% IoU).

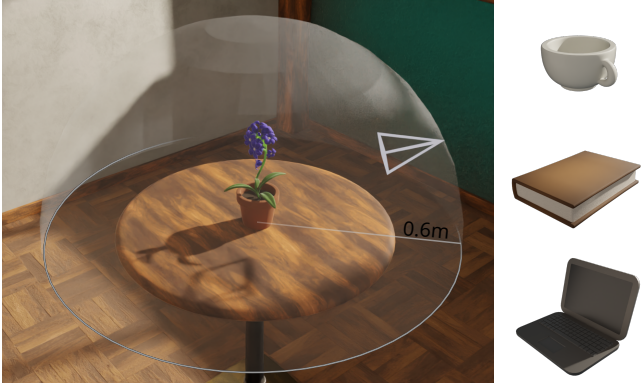


Fig. 6. The Blender Cube Diorama scene that is used in the baseline experiment, the instance noise experiment, and the pose error experiment. Training images are generated from a camera looking at the center of the table and placed on the sphere shown. The four table-top models “bluebell”, “laptop”, “book”, and “cup” are used to calculate confidence intervals.

**Results** Under ideal conditions, Figure 5 shows a reconstruction accuracy of 0.2 cm to 0.8 cm at 98% IoU can be achieved. Overall, increasing the number of images past a certain point has diminishing returns. Including a depth loss in the training results in an absolute increase in accuracy. Lastly, the farther away the image planes are from the object, the less accurate the reconstruction.

### B. Instance Noise

Instance masks are used to identify objects within an image. In contrast to synthetic scenes, masks output from MaskRCNN or other instance segmentation networks produce noisy output. The noise can be thought of as being applied in 2D. Therefore, masks of the same objects taken from different views are not consistent in the 3D world. In other words, rays that intersect an object at the same point may disagree on whether they should be classified as hitting the object or not. This experiment investigates how resilient NeRFs are to this kind of noise.

IoU is used as a measure of noise on the instance mask. Noise is introduced to an ideal mask by iteratively adding circular patches to the edge of the instance boundary until the IoU with the groundtruth is within 1% of the desired value.

Exemplary outputs from this method are shown in Figure 9. The experiment from section V-A is repeated with varying degrees of noise across the instance masks.

**Results** Figure 7 show that NeRFs are highly sensitive to noise in the instance masks. Increasing the number of images does not given an appreciable robustness to the noise. Adding depth supervision seems to give the NeRF more resilience. Figure 8 qualitatively shows the deterioration of the reconstruction.

### C. Camera Pose Errors

SLAM systems localize cameras with varying degrees of accuracy. We investigate how resilient NeRF training is to the noise. In this experiment, reconstruction quality is evaluated under increasing levels of perturbations to the camera poses. Rotation and translation inaccuracies are studied independently. Translation noise is introduced by adding a vector  $\eta \sim N(0, \text{diag}(\sigma_t^2, \sigma_t^2, \sigma_t^2))$  to the camera location. Rotation noise is introduced by twisting a camera pose about an arbitrarily chosen axis with an angle  $\theta \sim N(0, \sigma_r^2)$ .

Optimizing the camera poses as part of the training can cause a general drift in the poses. For example, if the poses drift upwards by 1 cm then the reconstruction itself is also shifted by 1 cm from the original coordinate frame. Consequently, the test set cannot be used for evaluation until the new coordinate frame is registered with the old one. To avoid this complication, we evaluate on the training set. This is an acceptable proxy because geometry formation is predominantly informed by color whereas the metric is derived from depth. The baseline experiment is repeated with pose noise applied.

**Results** Figure 10 shows that training on extrinsics gives a much needed robustness to localization errors. The NeRFs in our example can tolerate up to 2 cm of translation noise and 3 degrees of rotation error.

### D. Constrained Trajectory

Trajectories taken by a robot are unlikely to provide ideal coverage for objects of interest in a scene. Moreover, these objects are likely to exist within a cluttered environment. This further reduces the effectiveness of a collected training

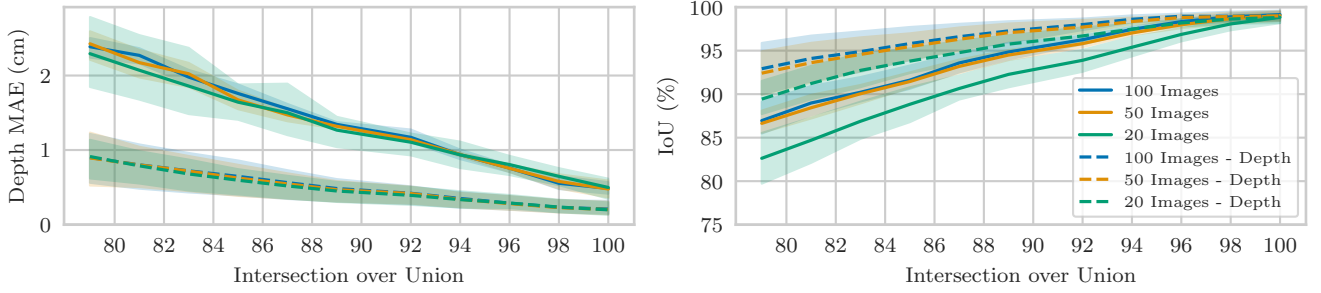


Fig. 7. Well-distributed images with groundtruth poses and noisy instance masks are used to reconstruct the same tabletop objects from the baseline experiment. The reconstruction quality deteriorates quickly with increasing noise levels. Depth supervision is more effective than increasing the number of training images at slowing the deterioration.

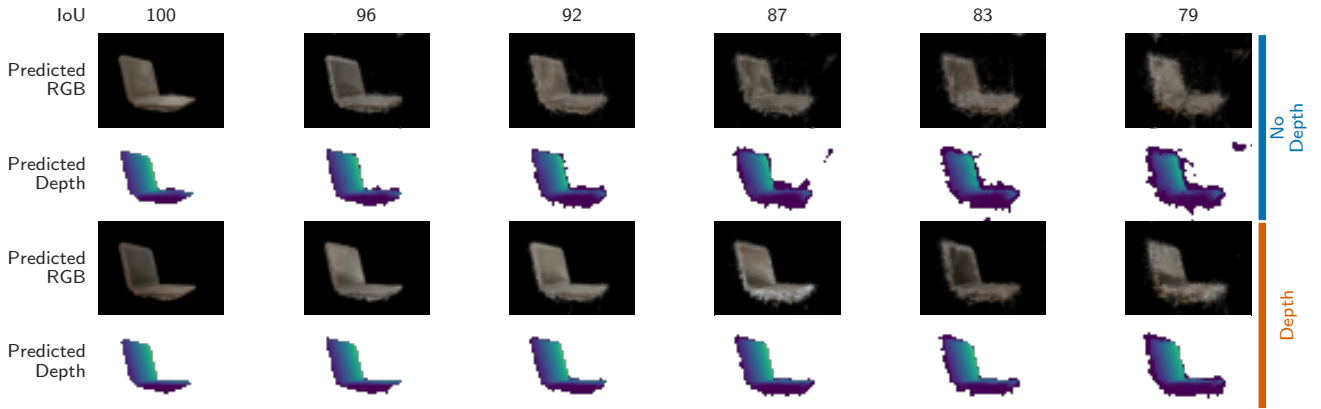


Fig. 8. A qualitative evaluation shows the sensitivity to instance mask noise. The silhouette of the object from a particular viewpoint deviates from its groundtruth with increasing noise levels indicating malformed geometry. Depth supervision alleviates the errors to some degree.

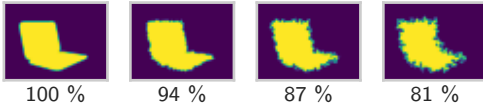


Fig. 9. Example outputs from the instance noise generator. This is used to controllably introduce noise into ideal instance masks and analyze its affect on the NeRF reconstruction. The numbers shown are the intersection-over-union of the resultant mask relative to the groundtruth.

set. For this experiment, the scene in Figure 11 is constructed with all four objects from Figure 6 placed together on a table. Images are sampled from a roughly circular trajectory instead of the ideal sphere. We examine how this constraint impacts the reconstruction under increasingly challenging scenarios. We use MaskRCNN [31] pre-trained on the MS-COCO dataset [33] to generate the instance masks. Furthermore, we use ORB-SLAM3 [29] to generate the poses. We evaluate on the training set for the same reasons given in section V-C.

**Results** As expected, Table II shows a robustness to noise in the camera poses with no appreciable drop in quality. Use of non-ideal instance masks results in a 7 to 12 percent drop in the IoU metric. This means thin structures will struggle to form under noisy instance masks as is also implied by the

TABLE II  
EFFECT OF NOISY DATA AND DEPTH SUPERVISION ON THE RECONSTRUCTION OF OBJECTS FROM A CONSTRAINED TRAJECTORY.

Masks	Depth	Poses	Depth MAE (cm)	IoU (%)
Ideal	True	Ideal	$0.5 \pm 0.3$	$98 \pm 1.5$
	True	ORB-SLAM	$0.6 \pm 0.3$	$98 \pm 0.6$
	False	Ideal	$1.1 \pm 0.3$	$98 \pm 0.8$
	False	ORB-SLAM	$1.4 \pm 0.3$	$98 \pm 1.1$
MaskRCNN	True	ORB-SLAM	$1.2 \pm 0.1$	$85 \pm 5.8$
		Ideal	$1.3 \pm 0.2$	$85 \pm 7.4$
	False	ORB-SLAM	$2.3 \pm 0.4$	$83 \pm 6.3$
		Ideal	$2.3 \pm 0.4$	$82 \pm 7.8$

real world experiment.

## VI. DISCUSSION

We developed a method that uses typical outputs from an object-based SLAM system to create a NeRF for each object found in a scene. The method was found to be robust to pose errors typical of SLAM systems. Furthermore, a constrained trajectory did not significantly affect the accuracy of the geometry observed by the cameras. We uncovered a sensitivity to noisy instance masks and found that incorporating more images into the training process alleviates the problems to some extent but has diminishing returns. Similarly, depth

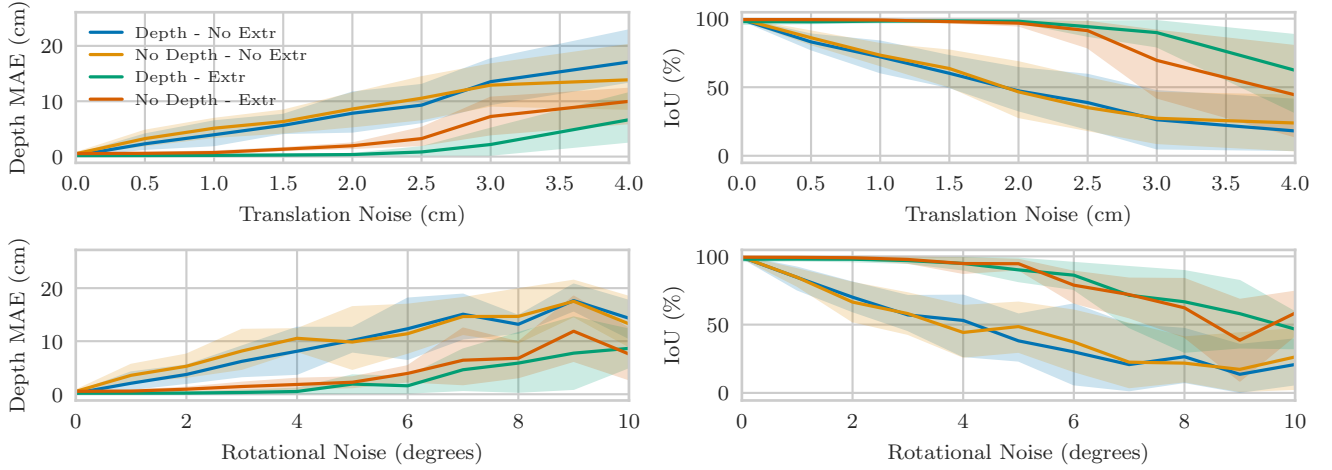


Fig. 10. Well-distributed images with ideal instance masks and inaccurate poses are used to reconstruct the same tabletop objects from the baseline experiment. Translation and rotation errors are treated separately. The resilience to either is shown when depth supervision is included and when the extrinsics are allowed to be optimized.



Fig. 11. Cluttered scene with a constrained trajectory. The primary image shows one of the training views with the overlaid instance masks detected by MaskRCNN. The secondary image shows a roughly circular trajectory that the camera takes.

supervision increased the robustness to mask noise in a well-distributed dataset. However, significant deterioration was still found in the constrained trajectory as is evidenced by the decrease in the IoU metric in Table II. This is likely because, in constrained trajectories, parts of the geometry always appear in the edges of the training images. The edges are the most susceptible to instance noise and we can expect the geometry around these areas to not form correctly. This makes forming thin structures especially difficult since they will always be near the edge of a mask.

This paper set out to extend object-based SLAM systems with an expressive geometric implicit representation. Baseline experiments showed that they can indeed provide a rich and accurate model. For the objects tested, a 4mm accuracy with 100% IoU can ideally be achieved. The issues of bounding and isolating objects from a scene was partially solved by our method through the use of instance masks and bounding boxes. However, the isolation process is not trivial. Given a set of instance masks that should agree in the 3D world but do not, what strategy should be used to minimise

the affect of the inconsistency? The method used relied on inconsistent rays cast through the NeRF to fight each other for dominance; hoping rays with true values would outnumber and overpower rays with false values. Results in Figure 7 do not indicate that this kind of “ray voting” occurs reliably and therefore finding a more robust procedure is an open problem.

Object-based SLAM systems are complimentary to NeRF representations. The localization they provide are accurate and fast enough for subsequent implicit mapping. The coarse primitives they use are an excellent means of bounding each object NeRF. This is a powerful advantage that other works [10], [20], [34] have not addressed as they rely on manually tuned parameters to limit the NeRF space. Though increasing the robustness of implicit representations to instance mask noise would yield better accuracy, our work still fills the gap between the austere representations of object-based SLAM systems and the expansive representations of scene-based NeRFs.

Object-based implicit representations are increasing the capabilities of mapping systems. They not only have an impressive ability to express geometric information but they can also be trained directly from images with minimal restrictive assumptions. It is foreseeable that manipulation and planning algorithms will evolve to leverage and consume the information provided by this new kind of representation. In doing so, they may usher a new phase of robotic capabilities.

## VII. CONCLUSIONS

NeRFs are exciting representations that can be used to extend current object-based SLAM systems. The two are structurally and functionally symbiotic. The object-based SLAM system creates bounding boxes around each object allowing a NeRF to be initialized with a proper scale. A NeRF, on the other hand, gives the much needed richness and accuracy that object-based SLAM systems fail to encode. In

this work, we saw that object NeRFs are robust to noise in the extrinsics but not robust to noise in the instance masks. Future work should address the ability of NeRFs to deal with this kind of noise which is characteristically not consistent in 3D.

## REFERENCES

- [1] E. Jang, C. Devin, V. Vanhoucke, and S. Levine, “Grasp2vec: Learning object representations from self-supervised grasping,” *arXiv preprint arXiv:1811.06964*, 2018.
- [2] W. Gao and R. Tedrake, “kpam-sc: Generalizable manipulation planning using keypoint affordance and shape completion,” in *2021 IEEE International Conference on Robotics and Automation (ICRA)*. IEEE, 2021, pp. 6527–6533.
- [3] J. Engel, T. Schöps, and D. Cremers, “LSD-SLAM: Large-scale direct monocular SLAM,” in *European Conference on Computer Vision (ECCV)*, September 2014.
- [4] T. Whelan, S. Leutenegger, R. F. Salas-Moreno, B. Glocker, and A. J. Davison, “Elasticfusion: Dense slam without a pose graph,” in *Robotics: Science and Systems*, 2015.
- [5] T. Whelan, M. Kaess, H. Johannsson, M. Fallon, J. J. Leonard, and J. McDonald, “Real-time large-scale dense rgb-d slam with volumetric fusion,” *The International Journal of Robotics Research*, vol. 34, no. 4-5, pp. 598–626, 2015.
- [6] L. Nicholson, M. Milford, and N. Sünderhauf, “Quadricslam: Dual quadrics from object detections as landmarks in object-oriented slam,” *IEEE Robotics and Automation Letters*, vol. 4, no. 1, pp. 1–8, 2019.
- [7] S. Yang and S. Scherer, “Cubeslam: Monocular 3-d object slam,” *IEEE Transactions on Robotics*, vol. 35, no. 4, pp. 925–938, 2019.
- [8] P. Erler, P. Guerrero, S. Ohrhallinger, N. J. Mitra, and M. Wimmer, “Points2surf learning implicit surfaces from point clouds,” in *Computer Vision – ECCV 2020*, A. Vedaldi, H. Bischof, T. Brox, and J.-M. Frahm, Eds. Cham: Springer International Publishing, 2020, pp. 108–124.
- [9] A. Simeonov, Y. Du, A. Tagliasacchi, J. B. Tenenbaum, A. Rodriguez, P. Agrawal, and V. Sitzmann, “Neural descriptor fields: Se (3)-equivariant object representations for manipulation,” *arXiv preprint arXiv:2112.05124*, 2021.
- [10] B. Mildenhall, P. P. Srinivasan, M. Tancik, J. T. Barron, R. Ramamoorthi, and R. Ng, “Nerf: Representing scenes as neural radiance fields for view synthesis,” in *European conference on computer vision*. Springer, 2020, pp. 405–421.
- [11] R. F. Salas-Moreno, R. A. Newcombe, H. Strasdat, P. H. Kelly, and A. J. Davison, “Slam++: Simultaneous localisation and mapping at the level of objects,” in *Proceedings of the IEEE conference on computer vision and pattern recognition*, 2013, pp. 1352–1359.
- [12] S. Yang and S. Scherer, “Monocular object and plane slam in structured environments,” *IEEE Robotics and Automation Letters*, vol. 4, no. 4, pp. 3145–3152, 2019.
- [13] J. J. Park, P. Florence, J. Straub, R. Newcombe, and S. Lovegrove, “DeepSDF: Learning continuous signed distance functions for shape representation,” in *Proceedings of the IEEE/CVF Conference on Computer Vision and Pattern Recognition*, 2019, pp. 165–174.
- [14] L. Mescheder, M. Oechsle, M. Niemeyer, S. Nowozin, and A. Geiger, “Occupancy networks: Learning 3d reconstruction in function space,” in *Proceedings of the IEEE/CVF Conference on Computer Vision and Pattern Recognition*, 2019, pp. 4460–4470.
- [15] V. Sitzmann, S. Rezkikov, W. T. Freeman, J. B. Tenenbaum, and F. Durand, “Light Field Networks: Neural Scene Representations with Single-Evaluation Rendering,” *arXiv:2106.02634 [cs]*, Jun. 2021, arXiv: 2106.02634. [Online]. Available: <http://arxiv.org/abs/2106.02634>
- [16] A. Yu, R. Li, M. Tancik, H. Li, R. Ng, and A. Kanazawa, “Plenotrees for real-time rendering of neural radiance fields,” in *arXiv*, 2021.
- [17] S. J. Garbin, M. Kowalski, M. Johnson, J. Shotton, and J. Valentin, “Fastnerf: High-fidelity neural rendering at 200fps,” <https://arxiv.org/abs/2103.10380>, 2021.
- [18] K. Deng, A. Liu, J.-Y. Zhu, and D. Ramanan, “Depth-supervised nerf: Fewer views and faster training for free,” *arXiv preprint arXiv:2107.02791*, 2021.
- [19] C. Sun, M. Sun, and H.-T. Chen, “Direct voxel grid optimization: Super-fast convergence for radiance fields reconstruction,” *arXiv preprint arXiv:2111.11215*, 2021.
- [20] T. Müller, A. Evans, C. Schied, and A. Keller, “Instant neural graphics primitives with a multiresolution hash encoding,” *arXiv:2201.05989*, Jan. 2022.
- [21] B. Yang, Y. Zhang, Y. Xu, Y. Li, H. Zhou, H. Bao, G. Zhang, and Z. Cui, “Learning object-compositional neural radiance field for editable scene rendering,” in *Proceedings of the IEEE/CVF International Conference on Computer Vision (ICCV)*, October 2021, pp. 13 779–13 788.
- [22] C. Xie, K. Park, R. Martin-Brualla, and M. Brown, “Fig-nerf: Figure-ground neural radiance fields for 3d object category modelling,” in *2021 International Conference on 3D Vision (3DV)*, 2021, pp. 962–971.
- [23] W.-C. Tseng, H. Liao, Y.-C. Lin, and M. Sun, “Cla-nerf: Category-level articulated neural radiance field,” *ArXiv*, vol. abs/2202.00181, 2022.
- [24] E. Sucar, S. Liu, J. Ortiz, and A. J. Davison, “iMAP: Implicit Mapping and Positioning in Real-Time,” *arXiv:2103.12352 [cs]*, Mar. 2021, arXiv: 2103.12352. [Online]. Available: <http://arxiv.org/abs/2103.12352>
- [25] Y. Li, S. Li, V. Sitzmann, P. Agrawal, and A. Torralba, “3d neural scene representations for visuomotor control,” in *Conference on Robot Learning*. PMLR, 2022, pp. 112–123.
- [26] L. Yen-Chen, P. Florence, J. T. Barron, T.-Y. Lin, A. Rodriguez, and P. Isola, “Nerf-supervision: Learning dense object descriptors from neural radiance fields,” *arXiv preprint arXiv:2203.01913*, 2022.
- [27] J. Ichnowski, Y. Avigal, J. Kerr, and K. Goldberg, “Dex-nerf: Using a neural radiance field to grasp transparent objects,” in *Conference on Robot Learning*. PMLR, 2022, pp. 526–536.
- [28] D. Driess, Z. Huang, Y. Li, R. Tedrake, and M. Toussaint, “Learning multi-object dynamics with compositional neural radiance fields,” *arXiv preprint arXiv:2202.11855*, 2022.
- [29] C. Campos, R. Elvira, J. J. G. Rodríguez, J. M. Montiel, and J. D. Tardós, “Orb-slam3: An accurate open-source library for visual, visual-inertial, and multimap slam,” *IEEE Transactions on Robotics*, vol. 37, no. 6, pp. 1874–1890, 2021.
- [30] D. P. Kingma and J. Ba, “Adam: A method for stochastic optimization,” *arXiv preprint arXiv:1412.6980*, 2014.
- [31] K. He, G. Gkioxari, P. Dollár, and R. Girshick, “Mask r-cnn,” in *Proceedings of the IEEE international conference on computer vision*, 2017, pp. 2961–2969.
- [32] B. O. Community, *Blender - a 3D modelling and rendering package*. Blender Foundation, Stichting Blender Foundation, Amsterdam, 2018. [Online]. Available: <http://www.blender.org>
- [33] T.-Y. Lin, M. Maire, S. J. Belongie, J. Hays, P. Perona, D. Ramanan, P. Dollár, and C. L. Zitnick, “Microsoft coco: Common objects in context,” in *ECCV*, 2014.
- [34] J. T. Barron, B. Mildenhall, M. Tancik, P. Hedman, R. Martin-Brualla, and P. P. Srinivasan, “Mip-nerf: A multiscale representation for anti-aliasing neural radiance fields,” in *Proceedings of the IEEE/CVF International Conference on Computer Vision*, 2021, pp. 5855–5864.